Journal of Materials Chemistry A

Accepted Manuscript

ROYAL SOCIETY OF CHEMISTRY

www.rsc.org/materialsA

Table of Content -- Manuscript ID TA-ART-12-2014-006856

Title: Probing the Initiation of Voltage Decay in Li-Rich Layered Cathode Materials

Authors: Yan Wu, Cheng Ma, Jihui Yang, Zicheng Li, Lawrence F. Allard, Chengdu Liang, and Miaofang Chi

Through a correlative investigation of electrochemical characterization and atomic-scale scanning transmission electron microscopy, the voltage decay in Li-rich layered cathode materials is found to originate between 4.4 and 4.8 V, and the most dramatic structural change associated is the layered-to-spinel transition that nucleates at the initial cycle.

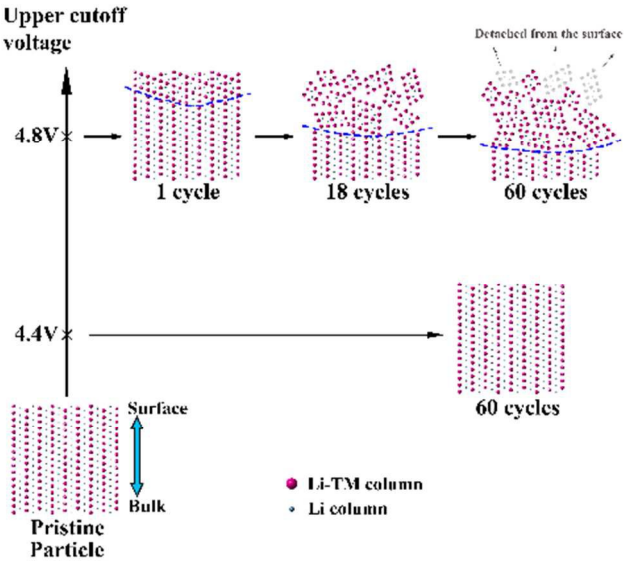

Journal of Materials Chemistry A

RSCPublishing

ARTICLE

Probing the Initiation of Voltage Decay in Li-Rich Layered Cathode Materials at Atomic Scale

Cite this: DOI: 10.1039/x0xx00000x

Received 00th January 2012,
Accepted 00th January 2012

DOI: 10.1039/x0xx00000x

www.rsc.org/

Yan Wu,[*,†,‡] Cheng Ma,[§,‡] Jihui Yang,[‖] Zicheng Li,[⊥] Lawrence F. Allard,[§] Chengdu Liang,[§] and Miaofang Chi[*,§]

Li-rich layered oxides hold great promise for improving the energy density of present-day Li-ion batteries. Their application is, however, limited by the voltage decay upon cycling, and the origin of such a phenomenon is poorly understood. A major issue is determining the voltage range over which the detrimental reactions originate. In the present study, a unique yet effective approach was employed to probe this issue. Instead of studying the material during the first cycle, the electrochemical behavior and evolution of the atomic structures were compared in extensively cycled specimens under varied charge/discharge voltages. With the upper cutoff voltage lowered from 4.8 to 4.4 V, the voltage decay ceased to occur even after 60 cycles. In the meantime, the material maintained its layered structure without any spinel phase emerging at the surface, which is unambiguously shown by the atomic-resolution Z-contrast imaging and electron energy loss spectroscopy. These results have conclusively demonstrated that the structural/chemical changes responsible for the voltage decay began between 4.4 and 4.8 V, where the layered-to-spinel transition was the most dramatic structural change observed. This discovery lays important groundwork for the mechanistic understanding of the voltage decay in Li-rich layered cathode materials.

Introduction

Rechargeable Li-ion batteries have revolutionized the industry of portable electronic devices, and are currently regarded as one of the most promising energy-storage technologies for enabling electric vehicles and smart grids.[1] However, these heavy-duty applications demand much higher energy density than that in the present generation of Li-ion batteries.[1] Among all the available options, adopting cathodes with a higher capacity is one of the most effective approaches for improving the energy density.[2] In this regard, the Li-rich layered oxides, (1-x)$LiMO_2$-xLi_2MnO_3 (M = Ni, Co, or Mn), are particularly attractive, as their capacity of ~250 mAh g^{-1} greatly surpasses those of all the other widely studied systems (which are typically lower than 200 mAh g^{-1}).[3] However, these compounds are plagued by severe voltage decay upon cycling.[4] Besides decreasing the energy density, this deleterious phenomenon causes difficulty in evaluating the state of charge of the battery, and thus raises safety concerns associated with overcharge.[4c] Such a drawback prevents practical applications of this high-capacity cathode material.[4]

The prerequisite for tackling the voltage decay issue is a mechanistic understanding of this phenomenon. The initial delithiation of (1-x)$LiMO_2$-xLi_2MnO_3 consists of two distinct steps.[3d, 4d, 5] In the first step, the charge compensation for the Li extraction is realized by oxidation of the M cations, which corresponds to a sloping region below 4.5 V in the voltage profile. Afterwards, the seemingly inactive Li_2MnO_3 component is activated via the removal of both Li and O, forming a plateau region above 4.5 V. While the voltage decay has been commonly assumed to relate to certain structural/chemical changes that initiate in this two-step

process,[4a, 4d, 6] the specific origin remains unclear. Many studies attribute the voltage decay to the development of a spinel phase during cycling, but the definitive evidence is still elusive.[6c] In addition, other phenomena, such as the migration of transition-metal (TM) cations into the Li sites at the particle surface[6c] and disruption of cation ordering,[7] *etc.*, were frequently speculated to contribute to the voltage decay. In order to identify the primary cause from all these possibilities, it is essential to know the exact voltage range where the detrimental effect initiates. However, the related studies are mainly focused on observing the structural evolution after full voltage range cycles, while the cause of such vulnarable voltage decay is still in strong debate. tThe most widely believed (although not yet conclusively cause for the voltage decay. According to the first-principles calculations and the associated structural analysis, the emergence of the spinel phase is facilitated by two structural changes during the initial charge:[6b] the formation of Li_{tet}–$V(TM)_{Li}$–Li_{tet} dumbbells (Li_{tet} and $V(TM)_{Li}$ refer to the Li at the tetrahedral site and Li vacancy in the transition-metal layer, respectively), and migration of transition-metal cations into the Li layer. Both of them occur in the sloping region (below 4.5 V) of the charge profile.[6b] However, it is also reported that the voltage decay behavior is governed by the plateau region (above 4.5 V);[4c] the compositions with a short plateau were found to exhibit much stable voltage profile. Furthermore, the oxidation of electrolytes and corrosion/fragmentation of particles have been observed to accompany the massive layered-to-spinel transition, implying the spinel phase could possibly be induced by an overly high cycling voltage (typically 4.8 V)[4a, 4c, 8] that is beyond the electrochemical window of the electrolyte (typically 1-4.7V[1a]).[6d, 9] Clearly the voltage range where the detrimental effect takes place cannot be conclusively identified based on the existing literatures.

The difficulty of probing this issue lies in the fact that the voltage decay is a cumulative phenomenon that would not become sufficiently significant for observation before a large number of cycles. As a result, the direct examination of the structure/chemistry at different stages of the first cycle can hardly provide conclusive insight into the voltage range where the relevant changes occur. Furthermore, the layered-to-spinel transition typically initiates at the surface of the particle, and, if the material is of high quality, the spinel layer would only be several nanometers thick even after extensive cycling. Such a localized nature makes the detailed study particularly challenging. In this study, we employed a unique approach to probe this issue. Instead of studying the material during the first cycle, we compared the electrochemical behaviors of the specimens that were extensively cycled under varied upper cutoff voltages. The associated structural/chemical evolutions were unravelled in the atomic scale via the state-of-the-art scanning transmission electron microscopy (STEM) and electron energy loss spectroscopy (EELS). These analyses pinpointed the voltage range where the key detrimental reactions occurred, and directly visualized the most dramatic structural change initiating in this voltage range. This is an important step towards understanding the voltage decay mechanism in the high-capacity Li-rich layered cathode material.

Results and discussion

An extensively investigated composition, $0.5LiMn_{1/3}Ni_{1/3}Co_{1/3}O_2$-$0.5Li_2MnO_3$ (equivalent to $Li_{1.2}Mn_{0.54}Ni_{0.13}Co_{0.13}O_2$), was selected for this study. When cycled at C/10 rate (the rate used in most studies), the material showed charge/discharge profiles (**Figure 1**a) consistent with those reported in literature.[4c, 9a, 10] Nevertheless, the evolution of the cell voltage cannot be straightforwardly learned from these curves, as the discharge capacity was also decreasing at this rate. In order to eliminate such a distraction, the material was cycled at a much slower rate of C/100 for the 1st and 60th cycles. As shown in Supporting Information Figure S1, the capacity barely changed, and a simple comparison between the two discharge curves unambiguously revealed obvious voltage decay. Although the voltage evolution in the charge/discharge curves at C/10 was obscured by the decreasing capacity, it can still be quantified via the nominal voltage. Figure 1b displays the nominal voltage *vs.* cycle number plot at C/10 rate. A continuous degradation of the voltage was immediately visible. After 60 cycles, the nominal voltage dropped from 3.61 to 3.05 V; only around 85% of the initial value was retained. Clearly the voltage decay always occurred regardless of the charge/discharge rate.

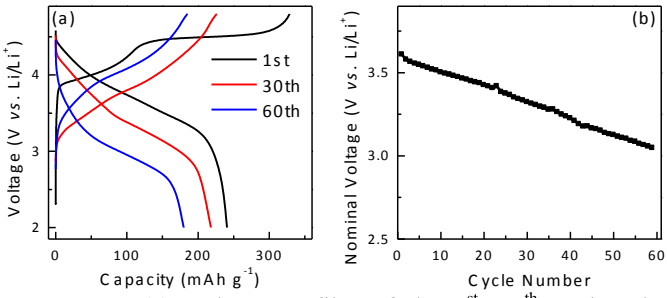

Figure 1. (a) Voltage profiles of the 1st, 30th, and 60th cycles. (b) Evolution of the nominal voltage during cycling. The cycling was performed at C/10 rate.

An in-depth understanding of the voltage decay phenomenon can be reached via scrutinizing the evolution of each redox reactions during cycling. **Figure 2** shows the dQ/dV plots of the electrochemical data at C/10. The discharge curve following the first charge to 4.8 V (Figure 2a) exhibited two peaks at around 3.5 and 3.75 V. The 3.75 V peak corresponded to the reduction of $Co^{4+/3+}$ and $Ni^{4+/3+/2+}$,[4b] which cannot be distinguished from each other in the plot, while the 3.5 V peak was associated with the reduction of $Mn^{4+/3+}$ in the activated Li_2MnO_3 (or MnO_2) component.[4b] During further cycling, an additional peak emerged at a voltage slightly lower than the $Mn^{4+/3+}$ reduction peak, forming a short plateau between 3.2 and 3.5 V in the dQ/dV curve (Figure 2c). While this peak was shifting towards lower voltages, its magnitude kept increasing at the expense of the other two peaks. At the 60th cycle (Figure 2e), the two reduction peaks of the layered phase were barely

visible; the discharge curve only showed a pronounced peak at around 3V, which was close to that was expected for a pure spinel.[4b, 11] This observation clearly suggested the layered-to-spinel transition was taking place gradually.[4b, 4d, 10] It should be noted that the layered phase should be present at the 60th cycle. Its presence was again obscured by the fast cycling rate. When the 60th cycle was performed at C/100, the reduction peak of the layered phase was still distinctly visible, residing in a lower voltage than that in the first discharge curve (Supporting Information Figure S2).

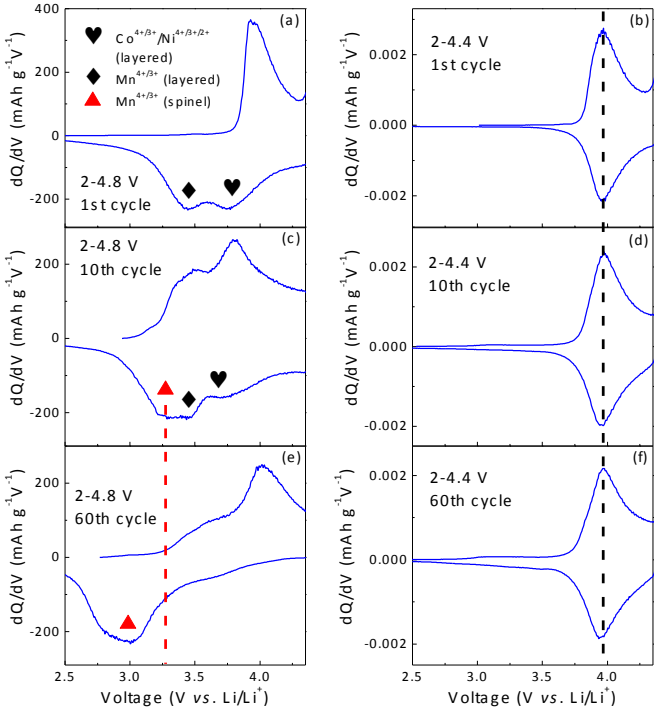

Figure 2. dQ/dV plots of the specimens cycled at C/10 rate between 2 and 4.8 V and those between 2 and 4.4 V.

In order to identify the voltage range that the structural/chemical changes are associated to the voltage decay, the material was cycled between 2 and 4.4 V. In this way, the charge/discharge of the $LiMn_{1/3}Ni_{1/3}Co_{1/3}O_2$ component was just complete, but the activation of Li_2MnO_3 has not yet initiated. The dQ/dV plots were displayed in Figure 2. In comparison with the specimen cycled between 2 and 4.8 V, the 2-4.4 V cycled specimen showed staggering differences. While the $Mn^{4+/3+}$ redox peaks in the layered phase no longer emerged due to the dormant Li_2MnO_3 component, neither the spinel redox peaks nor the voltage decay were observed upon repetitive cycling. The only peak in the dQ/dV curves was resulting from the $Co^{4+/3+}/Ni^{4+/3+/2+}$ redox reaction in the layered phase. Its position and shape remained largely unchanged even at the 60th cycle. This observation manifests that the essential cause of the voltage decay lied in certain reactions at the high-voltage region of 4.4-4.8 V.

The state-of-the-art (scanning) transmission electron microscopy [(S)TEM] and electron energy loss spectroscopy (EELS) analyses were performed to identify the structural/chemical changes showing the same dependence on the upper cutoff voltage. The results of the 2-4.8 V cycled specimen were shown in **Figure 3**. Figure 3a displays the high-

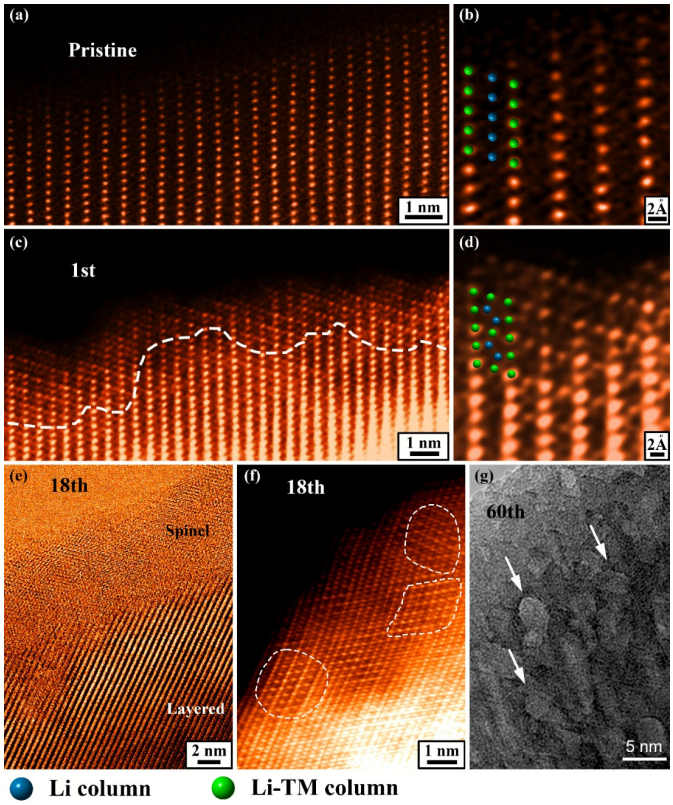

Figure 3. (a) HAADF-STEM image of a pristine particle along its [010] zone axis. (b) Surface of the particle in (a) at a higher magnification. (c) HAADF image of a particle along its [010] zone axis after one cycle. The surface region showing the spinel structure is delineated with dashed lines. (d) Surface of the particle in (c) at a larger magnification. Pure oxygen columns were omitted in the atomic models in (b) and (d) for clarification, and TM stands for "transition metal". (e) BF-STEM and (f) HAADF image of the surface of a particle after 18 cycles. Several regions showing different orientations to each other are delineated with dashed lines. (g) HRTEM image of a particle after 60 cycles. The detached pieces are indicated by white arrows.

angle annular dark-field (HAADF) image of a pristine particle along its [010] zone axis. With the image intensity dictated by the average atomic number,[12] a perfect layered structure can be straightforwardly identified. The arrays of brighter spots were the layer consisting of transition metal and Li cations, while the

in-between Li layers and oxygen columns did not contribute visible contrast due to the small atomic number (see overlaid atomic model in Figure 3b). After only one cycle between 2 and 4.8 V, visible contrast emerged in the Li layer in the outermost 3-4 unit cells at the surface (Figure 3c and d), and the resulted structure matched well with a standard spinel pattern (Figure 3d). During further cycling, the spinel phase kept growing at the expense of the layered phase. The thickness of the spinel layer increased from a few unit cells after one cycle to several nanometers after 18 cycles (Figure 3e). Accompanied with this was the continuously developing lattice strain between the bulk and surface. Consequently, nano-regions with different atomic configurations emerged in the surface spinel layer, and were readily developing into a polycrystalline structure. This was evidenced by the fast Fourier transformation (FFT) patterns from different regions of the spinel layer (Supporting Information Figure S3), and, more straightforwardly, the atomic-resolution HAADF image (Figure 3f). After 60 cycles, the surfaces generally became much rougher, preventing decent Z-contrast imaging at the atomic resolution. In addition, sponge-like regions were observed in most particles: the strain between certain spinel nano-grains and the surface must become so large that they detached from the particle (Figure 3h).

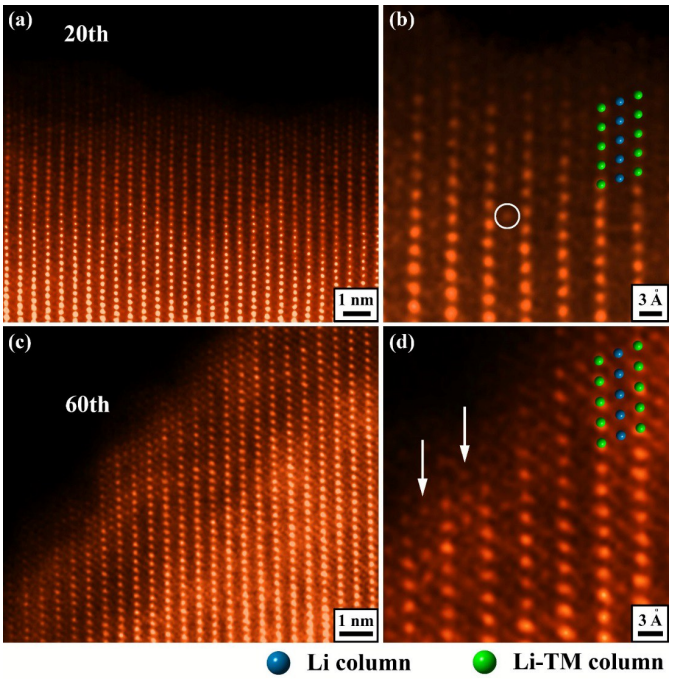

Figure 4. (a) HAADF image of a particle cycled between 2 and 4.4 V for 20 times. (b) Surface of the particle in (a) at a higher magnification. The bright circle highlighted a Li column that exhibited visible contrast due to the migration of transiton-metal cations into the Li layer. (c) HAADF image of a particle cycled between 2 and 4.4 V for 60 times. (d) Surface of the particle in (c) at a larger magnification. The Li layers containing transition-metal cations were indicated with bright arrows. All of these images were taken along the [010] zone axis. For clarification, the atomic models of the layered structure overlaid on (b) and (d) omitted the oxygen columns.

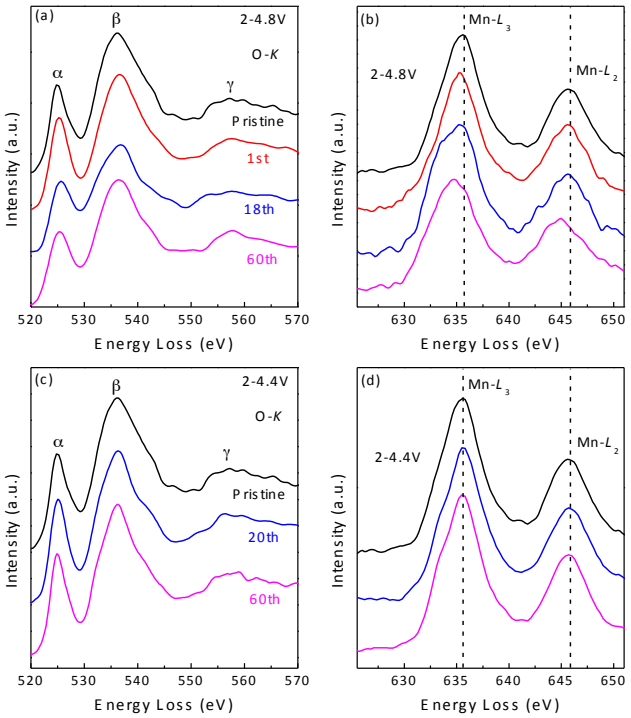

Figure 5. Evolution of the EELS spectra during cycling under different upper cutoff voltages.

With the upper cutoff voltage lowered from 4.8 to 4.4 V, not only the voltage decay was largely eliminated, but the development of the surface spinel phase also ceased to occur. **Figure 4**a displays the atomic-resolution HAADF-STEM image of a particle cycled between 2-4.4 V for 20 times. In sharp contrast to the 2-4.8 V cycled material (Figure 3e), the layered structure was preserved at the surface. Although faint spots symbolizing the transition-metal cations can occasionally be observed in the Li layer (Figure 4b), they were far from forming the typical spinel pattern shown in Figure 3. After 60 cycles (Figure 4c), the chance of observing transition-metal cations occupying the Li sites were slightly higher; certain Li layers at the outmost surface region (< 2nm) exhibited more than one atomic columns with visible contrast (marked by arrows in Figure 4d). Nevertheless, the amount of spinel phase, if any, was still negligibly small.

The dependence of the layered-to-spinel phase transition on the upper cutoff voltage was also corroborated by the EELS data (**Figure 5**). The EELS measurements were performed in 5nm×5nm regions to minimize the possible beam damage and include the contributions from both the surface and the bulk. For the specimens cycled between 2 and 4.8 V, the Co- and Ni-$L_{2,3}$ edges largely remained at the same position with increasing cycling number, but progressive changes were observed for the O-*K* and Mn-$L_{2,3}$ edges. As shown in Figure 5a, three

distinguished peaks were present in the O-*K* edge (labeled as α, β, and γ, respectively). Peak α was associated with the transitions of 1*s* electrons to the 2*p* states hybridized with TM 3*d* orbitals, while peaks β and γ originated from the mixing of the O 2*p* with *s* and *p* orbitals of Li and TM atoms. When the cycle number increased, peak α became less prominent in comparison with the other two peaks. This clearly suggested that the electronic environment of oxygen was modified, which was consistent with the emergence and growth of the spinel phase. Beyond this, more details in the chemical evolution can be perceived from the Mn-$L_{2,3}$ edge, which was caused by the transition of electrons from 2*p* to 3*d* orbitals and was very sensitive to the oxidation states of Mn. As shown in Figure 5b, both the L_2 and L_3 peaks were shifting towards lower energies with increasing the cycle number. This suggested Mn was slowly reduced during repetitive cycling.[13] Since the average valence state of transition-metal cations in the spinel structure is lower than that of Mn in $0.5Li(Mn_{1/3}Ni_{1/3}Co_{1/3})O_2$-$0.5Li_2MnO_3$ (3.5+ *vs*. 4+), the gradual reduction of Mn further supported the observed layered-to-spinel transition during cycling. In sharp contrast to the 2-4.8 V-cycled specimen, the 2-4.4 V-cycled materials did not exhibit any of the aforementioned EELS fine-structure evolutions (Figures 5c and d). Both the O-*K* and Mn-$L_{2,3}$ peaks largely remained unchanged even after 60 cycles. Therefore, the structural/chemical variation occurring in the 2-4.8 V-cycled specimen did not take place, which was in excellent agreement with both the electrochemical characterizations and HAADF-STEM observations.

A comprehensive comparison between the electrochemical data and microscopy results presented above can straightforwardly reveal an excellent correlation between the voltage decay and the layered-to-spinel transition. With the upper cutoff voltage lowered from 4.8 to 4.4 V, the voltage remained stable even after 60 cycles. In the meanwhile, the spinel phase ceased to emerge. Since the layered-to-spinel transition was the most substantial structural change between 4.4 and 4.8 V, it must contribute significantly to the voltage degradation. Furthermore, the fact that the spinel phase emerged only at high voltages implied it could be triggered by at least two possible factors. First of all, it could be the activation of Li_2MnO_3 component, which makes the redox reaction of $Mn^{4+/3+}$ participate in the cycling process. Mn^{3+} is a Jahn-Teller cation, but Mn^{4+} is not. As a result, severe local distortion can be expected in the redox reaction between them, which may induce the layered-to-spinel transition.[3e] The second possibility lies in the electrolyte. It is well known that the electrochemical window of the organic liquid electrolyte is typically 1-4.7 V.[1a] If the cathode is cycled beyond this range without an effective solid-electrolyte interphase (SEI) layer, it might oxidize the electrolyte. The identification of the root cause for the layered-to-spinel transition is beyond the scope of this study. Nevertheless, we did observe that the 2-4.4 V cycling after an initial activation to 4.8 V led to neither the voltage decay nor the spinel redox peaks in the dQ/dV plots (Supporting Information Figure S4). Finally, it should be pointed out that, although the layered-to-spinel transition, as the most dramatic crystal structure change during cycling, has been demonstrated to be closely correlated with the voltage decay, the possibility that other reactions were also contributing to the voltage decay should not be ruled out.

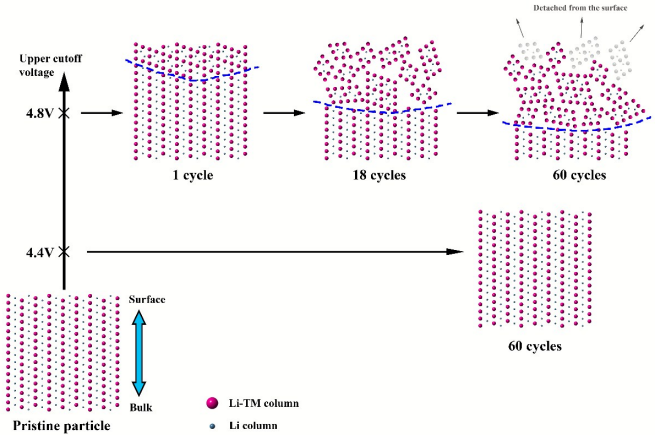

Figure 6. Schematic illustration of the dependence of the layered-to-spinel transition on the upper cutoff voltage.

A schematic illustration of these observations was presented in **Figure 6**. The voltage decay was found to be associated with the massive formation of spinel phases from the particle surface, and this phase transition exhibited a strong dependence on the cycling voltage. If the upper cutoff voltage was below 4.4 V, the particles would maintain its layered structure even after 60 cycles. Nevertheless, cycling beyond this voltage, *e.g.* 2-4.8 V, would induce the layered-to-spinel transition that degraded the voltage. After a limited number of cycles, only several outermost unit cells at the particle surface was transformed into the spinel structure. In the following cycles, this spinel phase kept growing in the consumption of the layered phase, and eventually developed into a polycrystalline structure to accommodate the strain between the bulk and the surface. With further cycling, the strain became so severe that some nanograins in the spinel layer began to detach from the surface. Because of the progressive formation of the spinel phase, the dQ/dV plots were gradually dominated by the low-voltage spinel peak, and thus decay in the nominal voltage was observed.

Conclusions

We have studied the voltage decay in the promising high-capacity cathode material $Li_{1.2}Mn_{0.54}Ni_{0.13}Co_{0.13}O_2$ under different cycling voltages. While the 2-4.8 V-cycled specimen showed severe voltage decay during cycling, the 2-4.4 V-cycled

one maintained a stable voltage even after 60 cycles. On the other hand, the layered-to-spinel transition occurring in the former specimen did not take place in the latter, as shown by the detailed atomic-scale structural/chemical analysis. These observations indicated that the detrimental reactions causing the voltage decay happened between 4.4 and 4.8 V, and also demonstrated that the most dramatic crystal structure change that initiated and developed in this voltage range was the layered-to-spinel transition. This is an important step towards understanding the voltage decay in Li-rich layered cathode materials.

Experimental Details

Chemical Synthesis: $Li[Li_{0.2}Mn_{0.54}Ni_{0.13}Co_{0.13}]O_2$ powders were synthesized by a co-precipitation method in which required amounts of the transition metal acetates ($Ni(CH_3CO_2)_2{\cdot}xH_2O$ (99+ %, Alfa Aesar), $Mn(CH_3CO_2)_2{\cdot}xH_2O$ (99+ %, Acros organics), $Co(CH_3CO_2)_2{\cdot}xH_2O$ (98+ %, Alfa Aesar)) were dissolved in deionized water and then added drop by drop into a 0.1 M KOH solution to form the co-precipitated hydroxides of Mn, Co, and Ni. The precipitates were filtered and washed with deionized water to remove any residual K^+ ions. After drying overnight at 100 ^oC in an oven (in air atmosphere), the co-precipitated hydroxides were mixed with 3% excess of the stoichiometry amount of lithium hydroxide and ground for half an hour, then fired in air at 900 ^oC for 24 h, and then cooled in air. The phase purity was verified by the x-ray diffraction.

Electrochemical Testing: 2032 coin cells were used for electrochemical testing. The cells used a lithium foil as the anode, 1 M $LiPF_6$ in ethylene carbonate (EC)/ diethyl carbonate (DEC) (1:2 vol.) as the electrolyte. Cathodes were prepared by mixing 75 wt.% active material with 20 wt.% acetylene black and 5 wt.% PTFE binder. All the cells were cycled galvanostatically at C/10 rate between different cutoff voltages at 30 °C.

TEM: TEM characterization was carried out on an aberration corrected FEI Titan 80/300 microscope equipped with a Gatan Quantum ER EELS spectrometer. The Z-contrast images were collected with a convergence semi-angle of 30mrad and inner collection semi-angle of 60mrad at 300kV. EELS spectra were acquired with a collection semi-angle of 50 mrad, and each spectrum presented in this paper is the sum of 40 spectra. Samples at different charged states were prepared by galvanostatically cycling at C/10 rate to the desired state of charge (SOC). The cell was then disassembled in an argon-filled glove box, and rinsed with dimethyl carbonate (DMC) to remove $LiPF_6$ salt. To minimize the exposure to air for the electrochemically charged/discharged samples, the TEM samples were prepared in an Ar environment and transferred to the microscope via vacuum transfer-system.

Acknowledgements

The microscopic work is supported by the in-house research of the Center for Nanophase Materials Sciences (CNMS), which is sponsored by the Scientific User Facilities Division. Collaborative work on the electrochemical analysis was supported by the U.S. Department of Energy, Office of Science, Materials Sciences and Engineering Division.

Notes and references

‡ These authors contributed equally to this work.

†General Motors Global R&D Center, 30500 Mound Rd. Warren, Michigan 48090, United States

§Center for Nanophase Materials Sciences, Oak Ridge National Laboratory, Oak Ridge, Tennessee 37831, United States

‖Department of Materials Science & Engineering, University of Washington, Seattle, Washington 98195, United States

⊥Optimal, Inc., Plymouth, Michigan 48170, United States

*Corresponding Authors

*E-mail: chim@ornl.gov

*E-mail: yan.wu@gm.com

Electronic Supplementary Information (ESI) available: Voltage profiles and dQ/dV plots of the 1st and 60th cycle between 2 and 4.8 V at C/100, FFT patterns from different regions of the spinel layer after 18 cycles between 2 and 4.8 V, dQ/dV plots of the 2-4.4 V cycled specimen after charging to 4.8 V in the initial cycle. See DOI: 10.1039/b000000x/

References

1. (a) Goodenough, J. B.; Kim, Y., Challenges for Rechargeable Li Batteries. *Chem Mater* **2010,** *22* (3), 587-603; (b) Thackeray, M. M.; Wolverton, C.; Isaacs, E. D., Electrical energy storage for transportation-approaching the limits of, and going beyond, lithium-ion batteries. *Energ Environ Sci* **2012,** *5* (7), 7854-7863.

2. (a) Tarascon, J. M., Key challenges in future Li-battery research. *Philosophical Transactions of the Royal Society a-Mathematical Physical and Engineering Sciences* **2010,** *368* (1923), 3227-3241; (b) Sathiya, M.; Ramesha, K.; Rousse, G.; Foix, D.; Gonbeau, D.; Prakash, A. S.; Doublet, M. L.; Hemalatha, K.; Tarascon, J. M., High Performance Li2Ru1-yMnyO3 (0.2 <= y <= 0.8) Cathode Materials for Rechargeable Lithium-Ion Batteries: Their Understanding. *Chem Mater* **2013,** *25* (7), 1121-1131.

3. (a) Lu, Z. H.; MacNeil, D. D.; Dahn, J. R., Layered cathode materials Li NixLi(1/3-2x/3)Mn(2/3-x/3) O-2 for lithium-ion batteries. *Electrochem Solid St* **2001,** *4* (11), A191-A194; (b) Lu, Z. H.; Dahn, J. R., Understanding the anomalous capacity of Li/Li NixLi(1/3-2x/3)Mn(2/3-x/3 O-2 cells using in situ X-ray diffraction and electrochemical studies. *J Electrochem Soc* **2002,** *149* (7), A815-A822; (c) Thackeray, M. M.; Johnson, C. S.; Vaughey, J. T.; Li, N.; Hackney, S. A., Advances in manganese-oxide 'composite' electrodes for lithium-ion batteries. *J Mater Chem* **2005,** *15* (23), 2257-2267; (d) Thackeray, M. M.; Kang, S. H.; Johnson, C. S.; Vaughey, J. T.; Benedek, R.; Hackney, S. A., Li2MnO3-stabilized LiMO2 (M = Mn, Ni, Co) electrodes for lithium-ion batteries. *J Mater Chem* **2007,** *17* (30), 3112-3125; (e) He, P.; Yu, H.; Li, D.; Zhou,

H., Layered lithium transition metal oxide cathodes towards high energy lithium-ion batteries. *J Mater Chem* **2012,** *22* (9), 3680-3695.

4. (a) Mohanty, D.; Kalnaus, S.; Meisner, R. A.; Rhodes, K. J.; Li, J. L.; Payzant, E. A.; Wood, D. L.; Daniel, C., Structural transformation of a lithium-rich Li1.2Co0.1Mn0.55Ni0.15O2 cathode during high voltage cycling resolved by in situ X-ray diffraction. *J Power Sources* **2013,** *229*, 239-248; (b) Croy, J. R.; Kim, D.; Balasubramanian, M.; Gallagher, K.; Kang, S. H.; Thackeray, M. M., Countering the Voltage Decay in High Capacity xLi(2)MnO(3)center dot(1-x)LiMO2 Electrodes (M=Mn, Ni, Co) for Li+-Ion Batteries. *J Electrochem Soc* **2012,** *159* (6), A781-A790; (c) Lee, E. S.; Manthiram, A., Smart design of lithium-rich layered oxide cathode compositions with suppressed voltage decay. *J Mater Chem A* **2014,** *2* (11), 3932-3939; (d) Johnson, C. S.; Li, N. C.; Lefief, C.; Vaughey, J. T.; Thackeray, M. M., Synthesis, Characterization and Electrochemistry of Lithium Battery Electrodes: xLi(2)MnO(3)center dot(1-x)LiMn0.333Ni0.333Co0.333O2 (0 <= x <= 0.7). *Chem Mater* **2008,** *20* (19), 6095-6106.

5. Boulineau, A.; Simonin, L.; Colin, J. F.; Canevet, E.; Daniel, L.; Patoux, S., Evolutions of Li1.2Mn0.61Ni0.18Mg0.01O2 during the Initial Charge/Discharge Cycle Studied by Advanced Electron Microscopy. *Chem Mater* **2012,** *24* (18), 3558-3566.

6. (a) Croy, J. R.; Gallagher, K. G.; Balasubramanian, M.; Chen, Z.; Ren, Y.; Kim, D.; Kang, S.-H.; Dees, D. W.; Thackeray, M. M., Examining Hysteresis in Composite xLi2MnO3·(1–x)LiMO2 Cathode Structures. *The Journal of Physical Chemistry C* **2013,** *117* (13), 6525-6536; (b) Xu, B.; Fell, C. R.; Chi, M. F.; Meng, Y. S., Identifying surface structural changes in layered Li-excess nickel manganese oxides in high voltage lithium ion batteries: A joint experimental and theoretical study. *Energ Environ Sci* **2011,** *4* (6), 2223-2233; (c) Boulineau, A.; Simonin, L.; Colin, J. F.; Bourbon, C.; Patoux, S., First Evidence of Manganese-Nickel Segregation and Densification upon Cycling in Li-Rich Layered Oxides for Lithium Batteries. *Nano Lett* **2013,** *13* (8), 3857-3863; (d) Zheng, J. M.; Gu, M.; Xiao, J.; Zuo, P. J.; Wang, C. M.; Zhang, J. G., Corrosion/Fragmentation of Layered Composite Cathode and Related Capacity/Voltage Fading during Cycling Process. *Nano Lett* **2013,** *13* (8), 3824-3830.

7. Mohanty, D.; Sefat, A. S.; Li, J.; Meisner, R. A.; Rondinone, A. J.; Payzant, E. A.; Abraham, D. P.; Wood Iii, D. L.; Daniel, C., Correlating cation ordering and voltage fade in a lithium-manganese-rich lithium-ion battery cathode oxide: a joint magnetic susceptibility and TEM study. *Phys Chem Chem Phys* **2013,** *15* (44), 19496-19509.

8. Yu, C.; Li, G. S.; Guan, X. F.; Zheng, J.; Luo, D.; Li, L. P., The impact of upper cut-off voltages on the electrochemical behaviors of composite electrode 0.3Li(2)MnO(3)center dot 0.7LiMn(1/3)Ni(1/3)Co(1/3)O(2). *Phys Chem Chem Phys* **2012,** *14* (35), 12368-12377.

9. (a) Yang, X. K.; Wang, D.; Yu, R. Z.; Bai, Y. S.; Shu, H. B.; Ge, L.; Guo, H. P.; Wei, Q. L.; Liu, L.; Wang, X. Y., Suppressed capacity/voltage fading of high-capacity lithium-rich layered materials via the design of heterogeneous distribution in the composition. *J Mater Chem A* **2014,** *2* (11), 3899-3911; (b) Robertson, A. D.; Bruce, P. G., Mechanism of electrochemical activity in Li2MnO3. *Chem Mater* **2003,** *15* (10), 1984-1992.

10. Zhao, T. L.; Chen, S.; Li, L.; Zhang, X. F.; Chen, R. J.; Belharouak, I.; Wu, F.; Amine, K., Synthesis, characterization, and electrochemistry of cathode material Li [Li0.2Co0.13Ni0.13Mn0.54]O-2 using organic chelating agents for lithium-ion batteries. *J Power Sources* **2013,** *228*, 206-213.

11. (a) Lee, E.-S.; Huq, A.; Chang, H.-Y.; Manthiram, A., High-Voltage, High-Energy Layered-Spinel Composite Cathodes with Superior Cycle Life for Lithium-Ion Batteries. *Chem Mater* **2012,** *24* (3), 600-612; (b) Lee, E.-S.; Huq, A.; Manthiram, A., Understanding the effect of synthesis temperature on the structural and electrochemical characteristics of layered-spinel composite cathodes for lithium-ion batteries. *J Power Sources* **2013,** *240* (0), 193-203.

12. Pennycook, S. J., Z-Contrast Transmission Electron-Microscopy - Direct Atomic Imaging of Materials. *Annu Rev Mater Sci* **1992,** *22*, 171-195.

13. Tan, H.; Verbeeck, J.; Abakumov, A.; Van Tendeloo, G., Oxidation state and chemical shift investigation in transition metal oxides by EELS. *Ultramicroscopy* **2012,** *116* (0), 24-33.